Astronomy & Astrophysics

Gamma-ray emission from Wolf-Rayet binaries

P. Benaglia[*] and G. E. Romero[*]

Instituto Argentino de Radioastronomía, C.C.5, (1894) Villa Elisa, Buenos Aires, Argentina

Abstract. In the colliding wind region of early-type binaries, electrons can be accelerated up to relativistic energies displaying power-law spectra, as demonstrated by the detection of non-thermal radio emission from several WR+OB systems. The particle acceleration region, located between the stars, is exposed to strong photon fields in such a way that inverse Compton cooling of the electrons could result in a substantial high-energy non-thermal flux. In particular cases, the ratio of the energy densities of magnetic to photon fields in the colliding wind region will determine whether a given source can produce or not significant gamma-ray emission. We present here a study of the binaries WR 140, WR 146, and WR 147 in the light of recent radio and gamma-ray observations. We show that with reasonable assumptions for the magnetic field strength WR 140 can produce the gamma-ray flux from the EGRET source 3EG J2022+4317. WR 146 and WR 147 are below the detection threshold, but new and forthcoming instruments like INTEGRAL and GLAST might detect non-thermal emission from them.

Key words. stars: early-type – stars: binaries: general – stars: winds, outflows – radio continuum: stars – gamma-rays: observations – gamma-rays: theory

1. Introduction

Early-type stars present strong supersonic winds that are responsible for significant mass loss rates, which in Wolf-Rayet (WR) stars can reach values close to 10^{-4} $M_\odot$ yr^{-1} (Abbott et al. 1986; Leitherer et al. 1997). These winds interact with the interstellar medium sweeping up the ambient material, creating cavities or bubbles (e.g. Benaglia & Cappa 1999), and forming strong shock fronts.

At the terminal shocks, with typical velocities of thousands of km s^{-1}, locally-injected supra-thermal particles could be accelerated up to relativistic energies and power-law distributions (e.g. Cassé & Paul 1980; Völk & Forman 1982). Energetic particles from the star lose too much energy in the expanding wind before reaching the shock to be efficiently accelerated, but it has been suggested that partial re-acceleration during their travel, produced by multiple shocks from line-driven instabilities in the inner wind region, could compensate the adiabatic losses (White 1985). In any case, if a continuous injection of supra-thermal protons or ions can be sustained, the subsequent interaction of the relativistic hadrons with ambient atoms will produce gamma-ray emission through the neutral pion chain: $p + p \to \pi^0 + X$, $\pi^0 \to \gamma + \gamma$.

For typical densities in the interstellar medium, however, the expected gamma-ray luminosity from isolated massive stars at energies $E > 100$ MeV is in the range 10^{32-33} erg s^{-1} (Benaglia et al. 2001), too low to be detected at standard distances, by instruments like the Energetic Gamma-Ray Experiment Telescope (EGRET) of the recently terminated Compton Gamma-Ray Observatory mission or even by the forthcoming AGILE Italian satellite (Mereghetti et al. 2001).

In the case of early-type binaries the situation is different. In a typical WR+OB binary the collision of the winds from both stars produces a strong shock at some point between the stars, in a region exposed to strong UV stellar fields. Both electrons and protons can be accelerated in these colliding wind regions (Eichler & Usov 1993). Electrons will cool through synchrotron and inverse Compton (IC) radiation. In fact, the detection of non-thermal radio emission in many early-type binaries corroborates the existence of a population of relativistic electrons in some of these systems (e.g. Dougherty & Williams 2000 and references therein). In some cases, like Cygnus OB2 No. 5, the colliding wind region is spatially resolved with VLA observations and it appears as an extended, lightly elongated non-thermal feature in the radio images (Contreras et al. 1997). In such cases, the geometry of the system can be established, radio flux components can be separated, and detailed calculations of the expected IC emission at high energies can be done. For the particular case of Cyg OB2 No. 5, for instance, Benaglia et al. (2001) estimate that about a half of the gamma-ray flux measured by EGRET from the Cyg OB2 association could come from the early-type binary.

Using data from the third and final EGRET catalog of point-like gamma-ray sources (Hartman et al. 1999), a correlation analysis between unidentified sources on the one hand and WR stars on the other shows several coincidences (Romero et al. 1999). The a priori chance probability is estimated in the

range 10^{-2}–10^{-3}, which is suggestive, but certainly not overwhelming as for the case of supernova remnants (Romero et al. 1999; Romero 2001). Some positional associations, however, deserve further study in the light of the most recent observations. This is particularly true for WR 140, a very interesting system whose possible high-energy emission has been already discussed in the pre-EGRET era by Pollock (1987) and also by Eichler & Usov (1993) in their seminal paper on non-thermal radiation from WR+OB binaries. The location of WR 140 is within the 98% confidence contour of the gamma-ray source 3EG J2022+4317. The existence of recent and detailed radio observations of this WR binary provides new tools for a reliable estimate of the expected gamma-ray flux, which can be now compared with the measured EGRET flux, not available at the time of Eichler & Usov's paper.

Physical conditions in WR binary systems with non-thermal colliding wind regions can be probed through gamma-ray observations. When thermal and synchrotron components of the radio emission can be adequately separated, the orbital parameters are well known, and the spectral types of the stars are determined, then the ratio of the synchrotron to the gamma-ray luminosity can be used to estimate the magnitude of the magnetic field in the shocked region. Even in case of a lack of clear gamma-ray detection, due to the instrument sensitivity, we can set bounds on the magnetic field strength, and hence make inferences on the field in the stars. The key point is that, granted the presence of a population of relativistic particles and an UV-photon field, both of which we know are present in WR binaries with non-thermal radio emission, then the production of IC gamma-rays is unavoidable. The question, of course, is whether these gamma-rays come with a flux density high enough as to be detected by the current technology.

In this paper we will study the case of three WR binaries: WR 140, WR 146, and WR 147. We will use the most recent results from radio observations in order to fix the value of model parameters, and then we will compute the expected gamma-ray luminosity with reasonable assumptions for the magnetic fields. We then will compare with gamma-ray observations in order to test our original assumptions. Finally, within the constrains imposed by the observations, we will make some predictions for gamma-ray instruments like INTEGRAL and GLAST.

We will not discuss cases of very close (i.e. short period) binary systems because they have typical separations of ∼0.1 AU, which impose an upper limit to the size of the particle acceleration region at the colliding wind shocks that results, in turn, in a severe constraint for the highest possible energy of the relativistic electrons. Even with strong magnetic fields of ∼1 Gauss in the shocked region, electrons could not go well within the GeV domain. However, soft gamma-rays of a few MeV are still possible, and some of these systems should deserve further high-energy studies as potential targets for the INTEGRAL satellite, which is optimized for such an energy range.

The structure of the paper is as follows. In the next section we will present the model for the gamma-ray emission from the colliding wind region. In Sect. 3 we will discuss the main characteristics of the WR binaries in our sample. Section 4 presents the existing gamma-ray information about the regions where the stars are located. In Sect. 5 we give the main results whereas in Sect. 6 we discuss some of their implications. We close in Sect. 7 with the conclusions.

2. Gamma-ray emission from massive binaries

Gamma-ray production in early-type binaries with colliding winds has been discussed by Eichler & Usov (1993), White & Chen (1995), Benaglia et al. (2001) and Mücke & Pohl (2002). We will present here the main features of the basic model.

In an early-type binary system the winds from the primary (e.g. a WR) and the secondary (e.g. an OB) stars flow nearly radially and collide at a point located at a distance r_i from the i-star, given by:

$$r_1 = \frac{1}{1 + \eta^{1/2}}D, \qquad r_2 = \frac{\eta^{1/2}}{1 + \eta^{1/2}}D. \tag{1}$$

In these expressions the subscript "1" stands for the primary star, and "2" for the secondary, D is the binary separation, and the parameter η is defined in terms of the wind terminal velocities v_∞ and the stellar mass loss rates $\dot{M}$:

$$\eta = \frac{\dot{M}_2 v_{\infty,2}}{\dot{M}_1 v_{\infty,1}}. \tag{2}$$

At the colliding wind region, first-order diffusive shock acceleration (e.g. Drury 1983) results in the production of a power-law spectrum $N(\gamma) \propto \gamma^{-p}$, with $p \simeq 2$ for electrons of energy $E = \gamma m_e c^2$. This is valid for particles with Lorentz factors $\gamma_{\min} \approx 2 < \gamma < \gamma_{\max}$. Because of the strong photon fields existing in the colliding wind zone, IC losses are expected to dominate the radiative cooling at high energies. The high energy cutoff of the electron spectrum can be then obtained from the condition that the IC loss rate for the particles does not exceed the acceleration rate (Eichler & Usov 1993):

$$\begin{aligned}
\gamma_{\max}^2 \simeq{}& 3 \times 10^8 \eta \left(\frac{v_{\infty,1}}{2 \times 10^8 \text{ cm s}^{-1}}\right)^2 \left(\frac{B}{\text{G}}\right) \\
&\times \left(\frac{D}{10^{13} \text{ cm}}\right)^2 \left(\frac{L_{\text{OB}}}{10^{39} \text{ erg s}^{-1}}\right)^{-1}.
\end{aligned} \tag{3}$$

Here B is the local value of the magnetic field and L_{OB} is the bolometric luminosity of the OB star, which is closer to the shock. Typical values for the maximum Lorentz factor are, according to Eq. (3), of a few times 10^4.

Inverse Compton losses will also produce a modification in the spectrum of the relativistic particles. A break is expected at the energy at which the cooling and escape times are equal (e.g. Longair 1997, p. 281). This will occur at a Lorentz factor γ_b given by:

$$\gamma_b = \frac{3m_e c}{4\sigma_T U t_{\text{esc}}}, \tag{4}$$

where U is the average energy density of the photon field, t_{esc} is average time spent by the particles in the field region (typically $t_{\text{esc}} \sim s/c$, with s the linear size of the colliding wind region), m_e is the electron mass, and σ_T the Thomson cross section. The spectrum will steepen from an index p to $p + 1$ for energies higher than γ_b.

The IC photons produced in a stellar photon field with seed photons of frequency $\nu_* = 5.8 \times 10^{10} T_{\text{eff}}$, where T_{eff} is the stellar effective temperature, are characterized by $\nu^{\text{IC}} = 4/3\gamma^2\nu_*$. The electrons will also lose energy through synchrotron emission in the magnetic field, producing a synchrotron flux with a spectrum $S(\nu) \propto \nu^{+\alpha}$, with $\alpha = (p-1)/2$. The frequency of the synchrotron photons will be $\nu_{\text{syn}} = 4.2 B \gamma^2$ MHz. Depending on the strength of the magnetic field, the tail of the synchrotron emission can reach even optical frequencies in some cases. Of course, in such bands it is not observable because of the overwhelming thermal contribution, but at radio wavelengths it can be detected and measured with interferometric instruments.

The rate of IC interactions in the colliding wind region per final photon energy is:

$$\frac{dN}{dt d\epsilon} = \frac{3\sigma_T c}{4\epsilon_0 \gamma^2} f(x), \qquad (5)$$

where ϵ_0 is the typical energy of the seed photons. For the case of Thomson scattering and adopting the "head-on" approximation (i.e. the photons – an isotropic field in the lab frame – are treated as coming from the opposite direction to the electron's velocity in the electron frame, see Jones 1968 for details), the function $f(x)$ can be written as:

$$f(x) = \frac{2}{3}(1-x)P(1/4\gamma^2, 1, x), \quad x = \frac{\epsilon}{4\epsilon_0\gamma^2}. \qquad (6)$$

This function P is such that $P = 1$ for $\frac{1}{4\gamma^2} < x < 1$ and $P = 0$ otherwise.

The specific luminosity is then obtained by integrating the scattering rate in Eq. (5) over the particle energy distribution, and multiplying by the observed photon energy ϵ and the number density $n_{\text{ph}} = U/\epsilon_0$. This leads to the expression:

$$
\begin{aligned}
L_\epsilon &= \frac{dL}{d\epsilon d\Omega} = \frac{kV\sigma_T m_e c^3}{8\pi\epsilon_0} \frac{U}{\epsilon_0} \frac{\epsilon}{\epsilon_0} \\
&\times \left\{ (\gamma_2)^{-(1+p)} \left(\frac{\epsilon}{4\epsilon_0(3+p)(\gamma_2)^2} - \frac{1}{1+p} \right) \right. \\
&\left. + \left(\frac{\epsilon}{4\epsilon_0} \right)^{-(1+p)/2} \frac{2}{(1+p)(3+p)} \right\}.
\end{aligned}
\qquad (7)
$$

Here, k is the constant involved in the energy distribution of the electrons, γ_2 the highest energy of the electrons considered in the calculation, and V the interacting volume. According to the energy range we are interested in, γ_2 can be equal to (or smaller than) γ_{max}. When p is steeper than 1 (as in our case) and $\gamma_{\text{min}} \ll \gamma_2$, this expression reduces to:

$$L_\epsilon = \frac{dL}{d\epsilon d\Omega} \approx \frac{kV\sigma_T m_e c^3}{\pi\epsilon_0(1+p)(3+p)} \frac{U 2^{p-1}}{} \left(\frac{\epsilon}{\epsilon_0} \right)^{-(p-1)/2}. \qquad (8)$$

A direct calculation of the IC luminosity of the colliding wind region of a particular binary system requires a knowledge of the parameter k in the electron energy distribution. This parameter is unknown, but we can use information on the synchrotron luminosity of these same electrons in order to circumvent this problem. In particular, the ratio of synchrotron to IC luminosities for the colliding wind region can be estimated as (White & Chen 1995; Benaglia et al. 2001):

$$\frac{L_{\text{syn}}}{L_{\text{IC}}} = 840 \frac{B^2 r_i^2}{L_i}, \qquad (9)$$

where B is expressed in G, r_i is the distance to the i-star in AU, and L_i is the star luminosity in $L_\odot$ units. Since L_{syn}, r_i, and L_i can all be, at least in principle, determined from observations, the gamma-ray visibility of the massive binary will crucially depend on the value of the magnetic field in the particle acceleration region.

It is usually assumed that the external magnetic field of the star in the absence of stellar wind is dipolar, and that with wind it obeys the standard $B \propto r^{-1}$ radial dependence for large r given by Eichler & Usov (1993):

$$B \approx B_* \frac{V_{\text{rot}}}{v_\infty} \frac{R_*^2}{r_A r} \quad \text{valid for } r > R_* \frac{v_\infty}{V_{\text{rot}}}, \qquad (10)$$

where R_* is the star radius, B_* the surface magnetic field, V_{rot} the surface rotational velocity, and $r_A \approx R_*$ the Alfvén radius. The value of the surface magnetic field is not well known, but it is thought that in WR stars could reach 10^4 G (e.g. Ignace et al. 1998). Then, in the colliding wind region of typical WR+OB binaries, the field could be in the range $10^{-2} - 10$ G.

At the colliding wind zone an equipartition magnetic field can be derived following Miley (1980):

$$B_{\text{eq}} = \left[\frac{2.84 \times 10^{-4}}{\theta_x \theta_y s (\sin\phi)^{3/2}} \frac{1+\chi}{f} \frac{F_o}{\nu_o^\alpha} \frac{\nu_2^{\alpha+1/2} - \nu_1^{\alpha+1/2}}{\alpha + 1/2} \right]^{2/7} \text{G.} \qquad (11)$$

Here θ_x, θ_y represent the source sizes in mas; χ is the energy ratio between heavy particles and electrons; f is the filling factor of the emitting region; s is the path length through the source in the line of sight, in AU; ϕ is the angle between the uniform magnetic field and the line of sight; F_0 the flux density in mJy of the region at frequency ν_0; and ν_1 and ν_2 are the upper and lower cut off frequencies presumed for the radio spectrum, these last three parameters expressed in GHz. For minimum energy conditions, $\chi = f = \sin\phi = 1$.

IC scattering of stellar photons is not the only mechanism capable of producing gamma-rays in the colliding wind region of an early-type binary. Relativistic bremsstrahlung in the ions of the winds will also result into gamma-ray emission. On the other hand, the same first-order acceleration mechanism that forms the electronic relativistic population should operate upon protons and ions. The decay of neutral pions generated in the hadronic interactions between the relativistic protons and the nuclei in the wind yields gamma-rays, which at high energies present the same energy spectrum than the parent proton population. At 67.5 MeV the spectrum should present the typical pion bump. All these complementary contributions, however, are rather minor in comparison with the IC emission because of the ambient densities involved in colliding wind binaries. In Sect. 5, when we will present the results of our calculations of the IC gamma-ray luminosity for several systems, we will also provide the expected bremsstrahlung and hadronic gamma-ray luminosities for completeness, but the reader is referred to Benaglia et al. (2001) and references therein for the formulae.

3. Selected binaries

The recently updated catalogue of WR stars (van der Hucht 2001) lists about 230 objects, all but one at distances up

Table 1. Wolf-Rayet stars with non-thermal – or combined – emission.

WR	Sp. Class.[a]	d (kpc)	Period[a] (days)	α[*]	Type	Observations (cm)
11	WC8 + O7.5III-V	0.26[a]	78.53	$[-0.5]$[b]	Comb	3, 6, 13, 20
14	WC7 + ?	2.00[a]	2.42	-1.0[b]	NT	3, 6
39	WC7 + OB?	5.53[a]	–	0.0[b]	Comb	3, 6, 13, 20
48	WC6(+O9.5/B0Iab)	2.27[a]	18.34	$-0.4, [-0.8]$[b]	NT	3, 6, 13
90	WC7	1.64[a]	–	0.0[b]	Comb	3, 6, 13
105	WN9h	1.58[a]	–	-0.3[b]	Comb	3, 6
112	WC9d + OB ?	4.15[a]	–	-1.35[b]	NT	3, 13
125	WC7ed + O9III	3.06[a]	>6600	$-0.5 \rightarrow 0.7$[c],[d]	Comb	2, 6, 20
137	WC7pd + O9	2.38[a]	4765	0.0[e]	Comb	1.6, 2, 3.7, 6
140	WC7pd + O4-5	1.10[a],1.3[f]	2900	-0.5[g],-0.6[h]	Comb	2, 6, 20
146	WC6 + O8	0.72[a],1.25[h]	ELPB[i]	-0.62[j]	RESOLVED	1.3, 3, 6, 20
147	WN8(h) + B0.5V	0.65[a]	ELPB[i]	-0.43[k],-1.1[l]	RESOLVED	1.3, 2, 3.6, 20

(*) Brackets mean non-thermal index derived from model; (a) van der Hucht (2001); (b) Chapman et al. (1999). (c) Abbott et al. (1986); (d) Williams et al. (1992); (e) Florkowski, private communication; (f) Smith et al. (1990). (g) White & Becker (1995); (h) van der Hucht et al. (2001); (i) stands for Extremely Long Period Binary. (j) Dougherty et al. (2000); (k) Setia Gunawan et al. (2001a); (l) Skinner et al. (1999).

to 20 kpc. Two main radio surveys with high-resolution have been carried out. The first one, using the VLA (Abbott et al. 1986) compiled data from ~40 stars up to 3 kpc, north of declination −47°. The southern one was done using ATCA (Leitherer et al. 1997; Chapman et al. 1999) and encompasses ~40 WR stars with $\delta < 0°$ and distances up to 3 kpc. Special objects were re-observed in recent years (e.g. Contreras et al. 1997; Dougherty et al. 1996, 2000, etc.). Some objects show spectral indices α approaching the canonical thermal value of +0.6, whereas the rest present negative and/or variable values.

For the present investigation, we looked first for candidates with detected non-thermal emission, indicating the presence of relativistic electrons. Taking into account the works mentioned above, a list can be made containing the objects that have shown spectral indices other than thermal. Such a list is presented in Table 1, where we have separated the stars in three groups or types, according to the spectral index: "Comb" sources are those that present an index near 0 or variable; "NT" ones have a clearly negative value of α. Two systems – WR 146 and WR 147 – have been "RESOLVED" using VLA and MERLIN in two sources each: one thermal, the other not. The spectral classification, distances, and periods in the table are taken mostly from van der Hucht (2001). Special references are given for the spectral indices. We also provide information on the different wavelengths at which the stars were detected.

After eliminating objects with no evidence of colliding winds or close binaries, we are left with WR 146 and WR 147 as the best candidates. The colliding wind region has been resolved in continuum radio observations for these systems. They have orbital periods of hundreds of years. The geometry of the colliding wind region is relatively clear for these binaries.

A third classical candidate was added to our sample: WR 140. Although the colliding wind region is not well-resolved here, this star has been monitored over its complete period, it has been pointed as the probable counterpart of an EGRET gamma-ray point source (Romero et al. 1999), and it was also the original example discussed by Eichler & Usov (1993) to illustrate their non-thermal model.

3.1. WR 140

WR 140 (HD 193793, V1687 Cyg) is a spectroscopic binary system, formed by a WC7pd and an O4-5 companion (van der Hucht 2001). It was the first star for which non-thermal emission has been detected (Florkowski & Gottesman 1977). The condition of colliding wind binary was confirmed by Williams et al. (1987), deducing a period of 7.9 yr and an eccentricity $e = 0.84$. It has shown variability at radio, IR, optical, UV, and X-rays (Setia Gunawan et al. 2001b and references therein). Periodic dust formation around periastron passage would be responsible for the IR excess observed (Williams et al. 1987).

Table 2. Stellar parameters adopted for the WR 140 system.

Variable	WR		OB	unit
Separation from colliding wind region	8.5[*]		1.5[*]	AU
Spectral Class.	WC7pd[a]		O4-5 (V)[b]	
$\log (L/L_\odot)$	5.35[c]		5.80[d]	
$T_{\rm eff}$	48 000[c]		47 400[d]	K
R_*	6.0[c]		12.0[d]	$R_\odot$
μ	5[c]		1.5[c]	
v_∞	2860[e]		3100[e]	km s^{-1}
$\dot{M}$	5.7×10^{-5}[e]		2.0×10^{-6}[c]	$M_\odot$ yr^{-1}
Distance d		1320[e]		pc
η		0.03		
Non-thermal spectral index α		-0.60[e]		
$S_{\rm 5\ GHz}$		22.5[e]		mJy
Size of non-thermal source s		6.0×10^{13}[c]		cm
Photon energy density U		38.5		erg cm^{-3}
$B_{\rm cwr}$ (equipartition)		200[c]		mG

(*) For binary separation of 10 AU; (a) van der Hucht (2001); (b) Setia Gunawan et al. (2001b). (c) adopted here, see text; (d) Vacca et al. (1996); (e) van der Hucht et al. (2001).

Both White & Becker (1995) and Williams et al. (1990, 1994) monitored the system at radio frequencies. The first authors used the VLA at 2, 6 and 20 cm, from 1985 to 1993. Williams et al. observed WR 140 from 1986 to 1994 with WSRT. The observations allow to estimate a spectral index of -0.6 (van der Hucht et al. 2001). They adopted a model in which the WR stellar wind is strongly enhanced at the equatorial plane, where most of the mass loss is confined. The emission suffers from varying circumstellar extinction in the line of sight to the non-thermal radio source that is identified with the colliding wind region. The orbit should be inclined. More recently, Setia Gunawan et al. (2001b) presented the results of 16 years of UV monitoring of WR 140, and provided explanations for the observed spectral variability.

The stellar parameters of WR 140 relevant to this work are listed in Table 2 along with the corresponding references. Throughout the period, the separation between the stellar components of the system ranges from 2.4 to 27 AU. We have assumed a separation $D = 10$ AU in order to compare with gamma-ray observations (see Sect. 4), and computed a value $\eta = 0.03$, that was used in our calculations (Sect. 5). The WR stellar luminosity was taken as an average of all model luminosities given by Koesterke & Hamann (1995) for WC7 stars. The luminosity class of the secondary is suggested by Setia Gunawan et al. (2001b) as O4-5(V). The effective temperature and radius of the primary were assumed the same of WR 125 (Koesterke & Hamann 1995), because of their similarities. The effective temperature, stellar luminosity, and radius for the secondary were taken from the tables of Vacca et al. (1996), for a spectral type O4.5 V. A mean molecular weight (μ) of 5 was adopted for the primary, and 1.5 for the secondary. The mass loss rate of the secondary was computed following the models of Vink et al. (2000).

Van der Hucht et al. (2001) give values for mass loss rates and wind terminal velocities of both components, the spectral non-thermal index, distance, and non-thermal flux density at 6 cm. In order to obtain an estimate of the extension of the colliding wind region, we have computed the radii of the photospheres at 5 GHz of both components, using the expression from Wright & Barlow (1975). After verifying they overlap, we have considered the size of the non-thermal source equal to the OB radio photosphere, about 4 AU. In all cases, the U value represents the sum of the photon energy density of each binary component, computed at the colliding wind region.

The equipartition magnetic field can be calculated with Eq. (11) using $\nu_1 = 1.4$ GHz and $\nu_2 = 250$ GHz (see Wendker 1995), and assuming a spherical non-thermal source with $\theta_x = \theta_y = 3$ mas, and $s = 4$ AU. Inaccuracies in the colliding wind region size or in the filling factor introduce the main errors in the determination of the magnetic field. For example, if $f = 0.1$, or $s = 2$ AU, the magnetic field doubles its value.

3.2. WR 146

This system contains the brightest WR star detected in radio continuum so far. The secondary is an OB star in an orbit with a period estimated in $\sim$300 yr (Dougherty et al. 1996).

After observing with the EVN and VLA, Felli & Massi (1991) detected emission with a spectral index $\alpha = -1$. Dougherty et al. (1996) resolved the system using MERLIN in two sources: a bright non-thermal northern component of 38 ± 1 mas in diameter, and a weaker southern component. Niemela et al. (1998) reported the resolution of the system after HST-WFPC2 observations. Their result for the binary separation was confirmed by 22 GHz observations taken by Dougherty et al. (2000), who detected the stellar wind of the companion star with the VLA. Their radio maps allowed to derive a value for r_2 of $\sim$50 AU, at $d = 1.25$ kpc, and $\eta = 0.1$. They took optical spectra of the system and interpreted the results as strongly suggesting that the O8 star is an Of, possibly a supergiant.

Setia Gunawan et al. (2000) presented the results of 1.4 and 5 GHz observations with WSRT, from 1989 to 1999.

Table 3. Stellar parameters adopted for the WR 146 system.

Variable	WR	OB	unit
Separation from colliding wind region	$160^{(*)}$	$50^{(*)}$	AU
Spectral Class.	WC6[a]	O8 If[b]	
$\log (L/L_\odot)$	$5.10^{(c)}$	$5.00^{(d)}$	
$T_{\rm eff}$	$49\,000^{(e)}$	$35\,700^{(f)}$	K
R_*	$5.0^{(e)}$	$23.1^{(f)}$	$R_\odot$
μ	$5.29^{(g)}$	$1.34^{(h)}$	
v_∞	$2700^{(g)}$	$1300^{(i)}$	km s^{-1}
$\dot{M}$	$2.6 \times 10^{-5(g)}$	$5.4 \times 10^{-6(d)}$	$M_\odot$ yr^{-1}
Distance d	$1250^{(i)}$		pc
η	0.10		
Non-thermal spectral index α	$-0.62^{(c)}$		
$S_{\rm 5\,GHz}$	$28.5^{(i)}$		mJy
Size of non-thermal source s	$7.0 \times 10^{14\ (d)}$		cm
Photon energy density U	6.1×10^{-3}		erg cm^{-3}
$B_{\rm cwr}$ (equipartition)	$25.0^{(d)}$		mG

(*) Deduced for $r_2 = 40 \pm 9$ mas (Dougherty et al. 2000); (a) Smith et al. (1990). (b) Dougherty et al. (2000); (c) Setia Gunawan et al. (2000); (d) adopted here, see text. (e) Koesterke & Hamann (1995); (f) Vacca et al. (1996); (g) Willis et al. (1997). (h) Lamers & Leitherer (1993); (i) van der Hucht et al. (2001).

They found three different kinds of flux variability behaviour on this time-span: a linear increasing trend observed during 10 years, a possible 3.38-yr periodic signal, and rapid fluctuations on time scales of weeks; they also derived a time-averaged non-thermal spectral index $\alpha = -0.62$.

The values adopted for our calculations are shown in Table 3. Since the distance estimates to the WR 146 binary system differ from 0.75 kpc to 1.7 kpc (Setia Gunawan et al. 2000 and references therein), we have carried out the calculations adopting the mean value $d = 1.25$ kpc (van der Hucht et al. 2001). The corresponding separation of the two stars is 210 AU (Setia Gunawan et al. 2000). The stellar luminosity of the secondary is an average of the values given by Setia Gunawan et al. (2000). The effective temperature and radius of the secondary were taken from the tables of Vacca et al. (1996). The mass loss rate of the secondary was computed from Eq. (2). The colliding wind region size was derived assuming an extension of the non-thermal source of 38 mas at 1.25 kpc (Setia Gunawan et al. 2000). We estimated the equipartition magnetic field between 327 MHz and 22 GHz (Taylor et al. 1996), with $\theta_x = \theta_y = 38$ mas, and $s = 46$ AU.

3.3. WR 147

Non-thermal emission form this system was reported after VLA observations by Abbott et al. (1986). Higher angular resolution observations taken with the same instrument (Churchwell et al. 1992) and MERLIN 5-GHz observations by Moran et al. (1989) confirmed the presence of two sources: a southern thermal one (WR 147S) superposed with the WR star, and a northern non-thermal component (WR 147N). Williams et al. (1997) observed the system again with MERLIN and found that the two sources are separated by 575 ± 15 mas. They reported also a faint IR source near WR 147N, but slightly farther to the WR star than the radio source WR 147N, and derived a spectral type B0.5 V for the IR star (confirmed later through optical observations by Niemela et al. 1998). Because of the presence of non-thermal emission between the two stars and its location much closer to the stars with the weaker wind, Williams et al. (1997) proposed the system as a colliding wind binary.

Using VLA observations at 3.6 cm, Contreras & Rodríguez (1999) found that the non-thermal wind-interaction zone remained constant in flux density during 1995-1996. The thermal emission from the WR star, on the contrary, increased $\sim 25\%$, probably reflecting the inhomogeneous nature of the wind. Both the observed radio morphology and the theoretical modeling by Contreras & Rodríguez (1999) clearly supports a colliding winds scenario for WR 147.

Setia Gunawan et al. (2001a) presented the results of a monitoring campaign of the source from 1988 to 1997 at 1.4 and 5 GHz with WSRT. Once subtracted the southern thermal contribution, the spectral energy distribution could be fitted by a synchrotron emission model which includes free-free absorption. Flux density variations on different time scales can be explained by considering inhomogeneities in the wind, plasma outflow, etc. After fitting the thermal source data, they computed a non-thermal flux density $S_{\rm NT} = S_{\rm total} - S_{\rm fit}$, obtaining the spectral indices $\alpha_{\rm thermal} = +0.6$ and $\alpha_{\rm syn} = -0.43$ for the thermal and synchrotron components, respectively. The statistical significance of this result, however, is very low. Skinner et al. (1999) have concluded, using nearly simultaneous observations at five frequencies, that there is a significant steepening in the non-thermal spectrum above 10 GHz. These authors have even suggested that a monoenergetic relativistic electron spectrum injected at the source might be a plausible explanation of the observed radio flux distribution. The quality of the radio data, unfortunately, does not allow to draw any firm conclusion.

Table 4. Stellar parameters adopted for the WR 147 system.

Variable	WR	OB	unit
Separation from colliding wind region	374[a]	43[b]	AU
Spectral Class.	WN8(h)[c]	B0.5 V[a]	
$\log (L/L_\odot)$	5.52[d]	4.70[e]	
$T_{\rm eff}$	26 000[d]	28 500[f]	K
R_*	20.6[e]	8.0[g]	$R_\odot$
μ	3.18[e]	1.5[b]	
v_∞	950[e]	800[b]	km s^{-1}
$\dot{M}$	2.4×10^{-5}[e]	4.0×10^{-7}[b]	$M_\odot$ yr^{-1}
Distance d	650[e]		pc
η	0.014		
Non-thermal spectral index α	-0.5[i]		
$S_{\rm 5\ GHz}$	12.5[h]		mJy
Size of non-thermal source s	2.6×10^{15}[b]		cm
Photon energy density U	4.0×10^{-3}		erg cm^{-3}
$B_{\rm cwr}$ (equipartition)	5.0[i]		mG

(a) Williams et al. (1997); (b) Setia Gunawan et al. (2001a), see text for a discussion; (c) Smith et al. (1996); (d) Crowther et al. (1995);
(e) Morris et al. (2000); (f) Crowther (1997); (g) Vacca et al. (1996); (h) van der Hucht et al. (2001); (i) adopted here, see text.

The parameters for the system WR 147 adopted in our calculations are listed in Table 4, with the respective references. A canonical value of $\alpha = -0.5$ was adopted, corresponding to the expected $p = 2$ spectrum in the electron distribution at relatively low energies. Compton losses will introduce a steepening at higher energies. In Sect. 6 we will revisit this assumption and we will briefly discuss the implications of the monoenergetic electron distribution suggested by Skinner et al. (1999) for the high-energy emission. The equipartition field at the colliding wind region was computed for $\theta_x = \theta_y = 267$ mas, and $s = 175$ AU, between frequencies 350 MHz (Setia Gunawan et al. 2001a) and 250 GHz (Wendker 1995).

4. Gamma-ray observations

The gamma-ray observations used here were provided by the EGRET telescope of the Compton satellite. The reduced data were published in the third EGRET catalog (Hartman et al. 1999). The catalog lists the best estimated position of 271 point gamma-ray sources, along with the location error boxes (taken as the 95% confidence contours), integrated gamma-ray fluxes in the energy range 100 MeV–20 GeV, spectral indices, and other information.

Only WR 140 is positionally coincident with a point-like source in the catalog, 3EG J2022+4317. The photon flux summed over satellite observing cycles 1, 2, 3, and 4 is $24.7 \pm 5.2 \times 10^{-8}$ ph cm^{-2} s^{-1}. The photon spectral index $F(E) \propto E^{-\Gamma}$ is $\Gamma = 2.31 \pm 0.19$. The location error box is large, with a radius of ~0.7 degrees, which renders a clear identification almost impossible in practice. However, WR 140 is the only highly energetic source known in this region (Romero et al. 1999). Figure 1 shows the relative position of WR 140 with respect to the gamma-ray source.

The EGRET viewing periods for this source cover since 1991 to 1994. Following the orbital positions and times
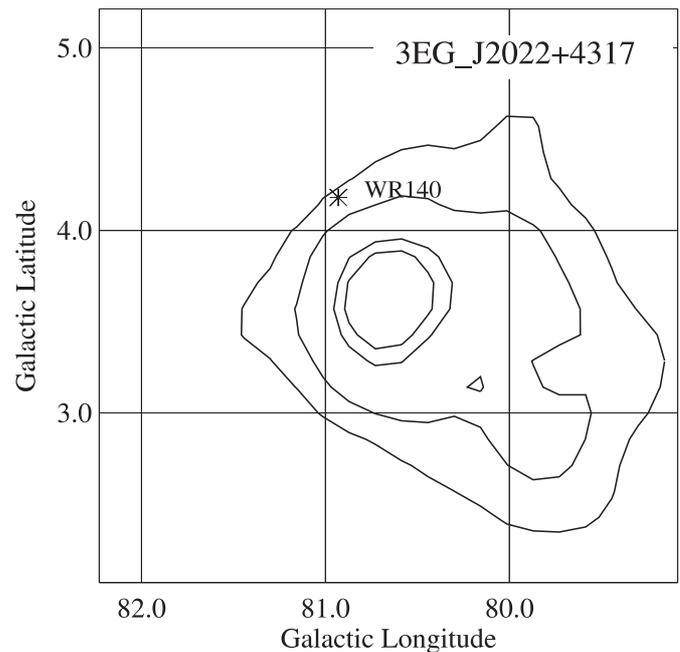
Fig. 1. EGRET probability contours for 3EG J2022+4317. Contour labels are 50% 68%, 95% and 98%. The position of WR 140 is marked.

deduced by Setia Gunawan et al. (2001b), the stars were separated between ~4 to ~16 AU during the time-span 1991.5–1994.5. We took a mean distance $D = 10$ AU for the binary separation during the gamma-ray observations in order to perform the calculations of the expected average flux.

The variability analysis of the gamma-ray data for 3EG J2022+4317 gives a variability index $I = 1.3$ in Torres et al. (2001a) scale, which is normalized to the average pulsar variability. A source will be variable if $I > 5$, at 8σ level. Non-variable sources have indices typically $I < 1.7$
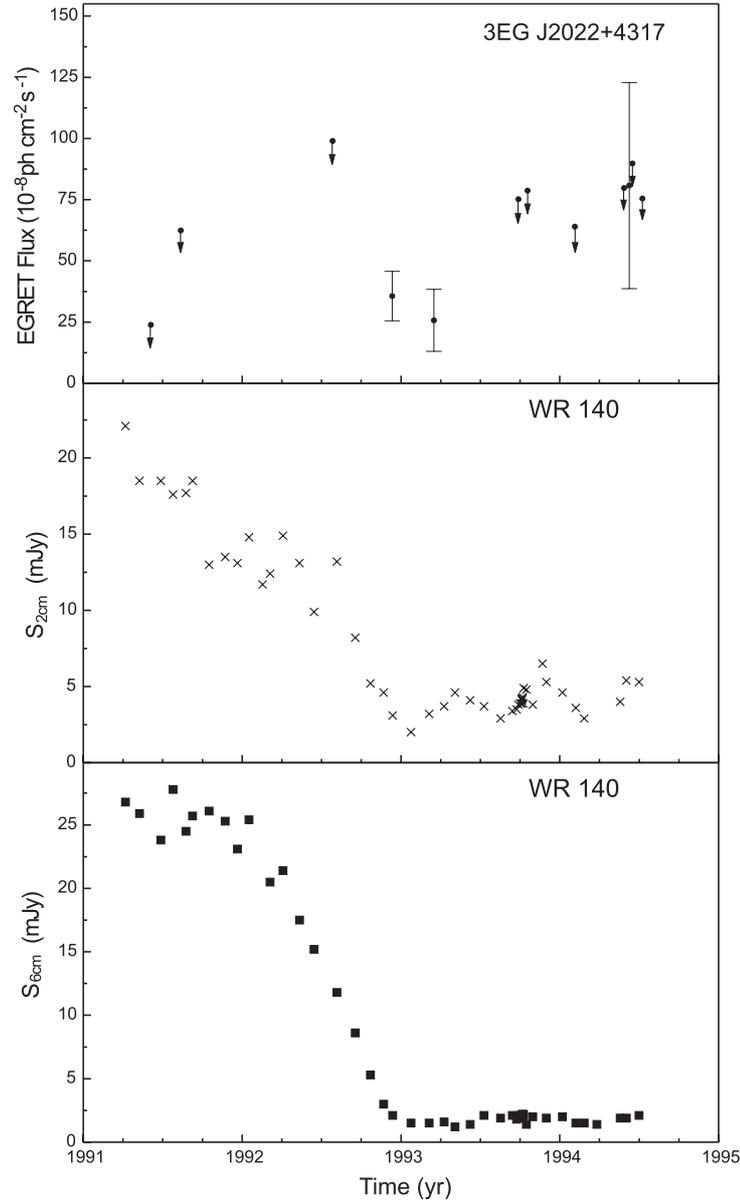
Fig. 2. Light curves at **a)** gamma-rays, **b)** 2 cm, and **c)** 6 cm.

(Torres et al. 2001b). Tompkins (1999) analysis yields for this source values of his τ index of $< \tau > = 0.13$, $\tau_{min} = 0.00$, and $\tau_{max} = 0.50$. Here, a variable source will have $\tau_{min} > 0.6$ (see Torres et al. 2001b for a comparison of both indices). Consequently, the source has not been formally variable during the observing time interval. But a note of caution is necessary here. As it can be seen in Fig. 2, upper panel, all but 3 observing periods for this source yielded only upper limits. In such a case the formal variability index can be misleading because under the upper limits real variability might be hidden. In the lower panels of Fig. 2 we show the radio evolution of the WR 140 for the same epoch of the gamma-ray observations. The data is taken from White & Becker (1995), directly from 1991 to 1993.6 and by extrapolation from 1993.6 to 1994.5. We can see that the radio flux was significantly decreasing from 1992 to 1993. If the value of the gamma-ray flux of the source was close to the upper limit established by EGRET

in mid-1992, then the high-energy emission might also have decreased significantly that year. The poor resolution of the EGRET lightcurve prevents any conclusion in this respect. It is not possible, in our opinion, to reject the association of WR 140 with 3EG J2022+4317 on the sole basis on the low variability indices.

Although the authors of the third EGRET catalog give the approximate upper limits for gamma-ray sources at almost any point in the sky, at the positions of WR 146 and WR 147 no threshold could be computed. The reason is that the positions of the stars are close to the fairly strong source 3EG J2033+4118. This makes it impossible for the gamma reduction programmes to get a statistically meaningful upper limit for weaker sources in the surroundings. Because of this contamination problem, we consider for the positions of WR 146 and WR 147, an EGRET detection limit of 70% of the flux of the gamma-ray source 3EG 2033+4118, i.e. 50×10^{-8} ph cm^{-2} s^{-1}, which

seems to be a reasonable assumption (Bob Hartman, private communication).

5. Results

The following results for the different WR binaries in our sample are obtained with the parameters listed in Tables 2–4. A summary of the results is presented in Table 5, where we list, for each system, the expected gamma-ray luminosity due to inverse Compton scattering, the relativistic bremsstrahlung, and the pion-decay contributions to the gamma-ray flux generated at the colliding wind region. In the following subsections we describe the main results of our calculations for each star.

5.1. WR 140

For this system we have $B_{cwr} \sim 0.2$ G and a very high photon energy density of $U = 38.5$ erg s^{-1}. The inverse Compton losses impose an upper energy limit for the locally accelerated electrons of $\gamma_{max} = 4 \times 10^4$ and a break in the spectrum at $\gamma_b \approx 400$. The break will appear in the synchrotron spectrum at $\nu_{b,\,syn} \approx 135.2$ GHz and at gamma-ray energies at $E_b = 2.45$ MeV, below the EGRET energy range. The Lorentz factors of electrons radiating IC gamma-rays in the ambient photon fields and contributing to 100 MeV$-$20 GeV are between $\gamma_1 = 2.5 \times 10^3$ and $\gamma_2 = 3.6 \times 10^4$. Electrons having Lorentz factors in this range are also capable of emitting synchrotron radiation between $\nu_1 = 5.5 \times 10^3$ GHz and $\nu_2 = 1.1 \times 10^6$ GHz. The total synchrotron luminosity from these electrons is $\sim 2.5 \times 10^{30}$ erg s^{-1}.

The total gamma-ray luminosity due to IC scattering at the colliding wind region between 100 MeV and 20 GeV results $\sim 2.1 \times 10^{34}$ erg s^{-1}. At this energies, after the break in the gamma-ray spectrum, the photon spectral index should be $\Gamma \sim 2.1$ (original injection spectrum with $p = 2.2$ according to radio observations below the break). Such an index is in reasonable agreement with the index observed by EGRET in the source 3EG J2022+4317 ($\Gamma = 2.31 \pm 0.19$), especially if we take into account that there are also uncertainties in the determination of the radio spectral index.

Both the luminosities due to pion decays from $p - p$ interactions ($<10^{22}$ erg s^{-1}) and relativistic bremsstrahlung in the winds ($<10^{32}$ erg s^{-1}) can be disregarded in comparison to the IC luminosity (see Benaglia et al. 2001 for details of calculation).

If the unidentified gamma-ray source 3EG J2022+4317 is at the same distance of WR 140, the measured EGRET flux implies a luminosity of $\sim 3.2 \times 10^{34}$ erg s^{-1}, of the same order of magnitude than the computed luminosity due to IC scattering at the colliding wind region. Errors in the observed gamma-ray emission are at the level of $\sim 25\%$. An additional factor that can affect the computations is the luminosity of the secondary star. For the WR 140 system it is not derived directly from observations, but interpolated from the tables of Vacca et al. (1996) and can be slightly overestimated. In any case, it seems likely that significant part of the gamma-ray flux of 3EG J2022+4317 might be contributed by the colliding wind region of WR 140.
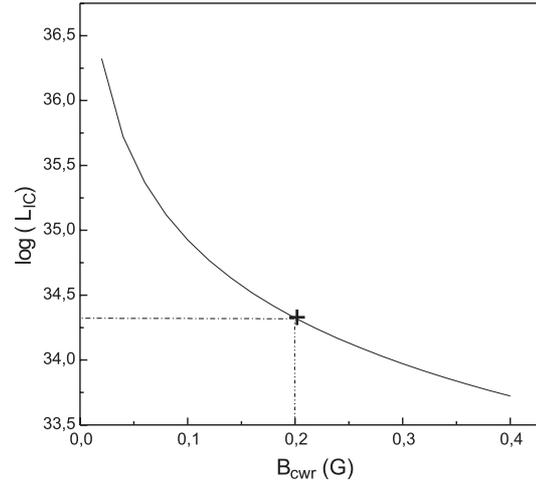
Fig. 3. Gamma-ray luminosity (in erg s^{-1}) between 100 MeV and 20 GeV versus the magnetic field for WR 140. The horizontal line indicates the expected luminosity of 3EG J2022+4317, if it is located at the distance of WR 140.

In Fig. 3 we present a plot of the gamma-ray luminosity of the colliding wind region of WR 140 versus the assumed magnetic field. The luminosity of 3EG J2022+4317 at the same distance is indicated with a horizontal line. For high values of the magnetic field the synchrotron losses dominate over IC losses, and the gamma-ray emission is quenched. We emphasize, however, that in order to explain the gamma-ray source 3EG J2022+4317 through WR 140, no extreme hypothesis is required, and the Occam's razor principle is fulfilled since no new and otherwise yet undetected object is postulated. In this sense, we suggest that WR 140 should be considered as the best currently available explanation for the origin of 3EG J2022+4317. The GLAST telescope, with its improved source location accuracy, will be able to test this proposition.

5.2. WR 146

For this system the equipartition magnetic field is significantly lower than in the case of WR 140: $B_{cwr} \sim 25$ mG. This lower value is mainly due to the different size and location of the non-thermal regions. With the values of the parameters listed in Table 3, we obtain the following results.

The maximum energy of the accelerated particles in the colliding wind region is $\gamma_{max} = 6 \times 10^5$. These are very energetic particles indeed. At such energies Klein-Nishima effects are important. The highest energy for IC photons produced by these electrons is $\sim \gamma_{max} m_e c^2 / 2 \sim 0.2$ TeV.

The Lorentz factors of the electrons contributing to EGRET's energy range are between $\gamma_1 = 3 \times 10^3$ and $\gamma_2 = 4.2 \times 10^4$. The local energy density $U = 6.1 \times 10^{-3}$ erg cm^{-3} implies a break in the spectrum at very high energies, within the optical region (4.9×10^6 GHz). Electrons having Lorentz factors in the above range radiate synchrotron photons between $\nu_1 = 9.2 \times 10^2$ GHz and $\nu_2 = 1.8 \times 10^5$ GHz. The total synchrotron luminosity in this frequency range is 3.3×10^{31} erg s^{-1}.

The gamma-ray luminosity due to IC scattering at the colliding wind region, contributed by seed photons from both stars
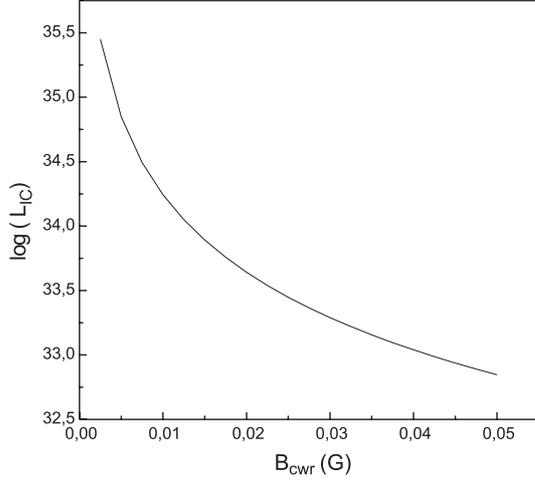
Fig. 4. Gamma-ray luminosity (in $\mathrm{erg\,s^{-1}}$) between 100 MeV and 20 GeV versus the magnetic field for WR 146.

Fig. 5. Gamma-ray luminosity (in $\mathrm{erg\,s^{-1}}$) between 100 MeV and 20 GeV versus the magnetic field for WR 147.

is $\sim 2.8 \times 10^{33}$ $\mathrm{erg\,s^{-1}}$. In comparison, the gamma-ray luminosity due to pion decay is $\sim 2.5 \times 10^{21}$ $\mathrm{erg\,s^{-1}}$, and to relativistic bremsstrahlung, $\sim 4.6 \times 10^{29}$ $\mathrm{erg\,s^{-1}}$, resulting both negligible. The IC spectral break appears at high energies (538 GeV), well above EGRET's range, so the spectrum in the MeV–GeV band should be much harder than in the case of WR 140, with values $\Gamma \sim 1.6$.

Figure 4 presents a plot of the gamma-ray luminosity between 100 MeV and 20 GeV versus the magnetic field. Very weak fields are ruled out by the EGRET non-detection.
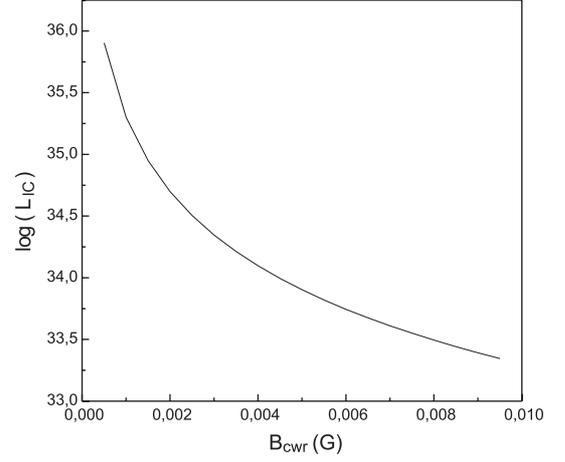
As we mentioned, the EGRET threshold towards the position of WR 146 can be taken as 50×10^{-8} $\mathrm{ph\,cm^{-2}\,s^{-1}}$. This means that a gamma-ray source at the distance of the binary system would be detectable by EGRET if its luminosity is greater than 8.0×10^{34} $\mathrm{erg\,s^{-1}}$, which is more than an order of magnitude above the expected luminosity coming from the colliding wind region. This fact can explain why no gamma-ray source was detected towards WR 146. However, as we will see, the expected flux is high enough as to be detected by GLAST, if the contamination problem from nearby sources can be solved.

5.3. WR 147

For WR 147 we have $B_{\mathrm{cwr}} \sim 5$ mG. The maximum Lorentz factor for the electrons imposed by the IC losses is $\gamma_{\mathrm{max}} = 1.0 \times 10^5$. The high-energy cutoff frequency is then $\nu_{\mathrm{cutoff}} = 2.1 \times 10^{25}$ Hz or ~ 90 GeV.

The Lorentz factors of the electrons whose IC emission falls in EGRET's energy range are between $\gamma_1 = 3.3 \times 10^3$ and $\gamma_2 = 4.7 \times 10^4$. Their synchrotron radiation is between $\nu_1 = 230$ GHz and $\nu_2 = 4.6 \times 10^4$ GHz. The total synchrotron luminosity with such frequency interval results $\sim 5.7 \times 10^{30}$ $\mathrm{erg\,s^{-1}}$. The break produced by the local photon field of density $U = 4.0 \times 10^{-3}$ $\mathrm{erg\,cm^{-3}}$ in the electron spectrum occurs at a Lorentz factor of $\gamma_{\mathrm{b}} \approx 8.9 \times 10^4$, and results in breaks in the synchrotron (at $\sim 1.7 \times 10^5$ GHz) and IC spectrum (at ~ 72 GeV).

The gamma-ray luminosity due to IC scattering at the colliding wind region, contributed by both stars, is

$\sim 8.0 \times 10^{33}$ $\mathrm{erg\,s^{-1}}$. In Fig. 5 we show how this luminosity would change with the assumed magnetic field. The gamma-ray luminosity due to pion decay is $\sim 1.0 \times 10^{23}$ $\mathrm{erg\,s^{-1}}$ and the corresponding to relativistic bremsstrahlung, $\sim 4.7 \times 10^{29}$ $\mathrm{erg\,s^{-1}}$.

The EGRET threshold towards the position of WR 147 is similar to that for WR 146. A gamma-ray source at the distance of the binary system would have been detected by EGRET if its luminosity is greater than 2.2×10^{34} $\mathrm{erg\,s^{-1}}$, i.e. more than a factor two above the expected level of WR 147, according to the estimates based on the parameters in Table 4. As for WR 146, this fact could explain why no gamma-ray source was found yet towards WR 147.

6. Discussion

6.1. Stellar magnetic fields and the Razin–Tsytovich effect

The magnetic field on the star surface can be computed using Eq. (10) and the magnetic fields estimated for the particle acceleration regions in Sect. 5.

The rotational velocity is not well determined for the binaries selected here. We consider typical values of 400 $\mathrm{km\,s^{-1}}$ for the WR stars, and the Alfvén radius $r_{\mathrm{A}} \sim R_*$. The resulting values for the surface stellar fields are given in Table 6 as B_*. They are between ~ 50 and 1200 G, in accordance with typical values estimated by Maheswaran & Cassinelli (1994) for WR stars.

If the magnetic field is much stronger, then WR 140 would fall below EGRET sensitivity. On the other hand, as indicated by White & Chen (1995), if the field is much weaker, the Razin–Tsytovich effect would suppress the observed synchrotron emission at cm wavelengths. The frequency at which the radiation is suppressed is:

$$\nu_{\mathrm{R}} \simeq 20\,\frac{n_{\mathrm{e}}}{B}\ \mathrm{Hz}, \tag{12}$$

Table 5. Gamma-ray production in the colliding wind regions of WR 140, WR 146, and WR 147, for the energy range 100 MeV $< E <$ 20 GeV.

Stellar system	Mechanism	Expected luminosity (erg s^{-1})	Observed luminosity or upper limit[1] (erg s^{-1})
WR 140	Inverse Compton scattering	$\sim 2.1 \times 10^{34}$	
	Relativistic bremsstrahlung	$\sim 1.3 \times 10^{31}$	$\sim 3.2 \times 10^{34}$
	Neutral pion decay	$\sim 1.2 \times 10^{21}$	
WR 146	Inverse Compton scattering	$\sim 2.8 \times 10^{33}$	
	Relativistic bremsstrahlung	$\sim 4.6 \times 10^{29}$	$< 8.0 \times 10^{34}$
	Neutral pion decay	$\sim 2.5 \times 10^{21}$	
WR 147	Inverse Compton scattering	$\sim 8.0 \times 10^{33}$	
	Relativistic bremsstrahlung	$\sim 4.7 \times 10^{29}$	$< 2.2 \times 10^{34}$
	Neutral pion decay	$\sim 1.0 \times 10^{23}$	

[1] From EGRET observations and assuming the gamma-ray sources at the same distances of the stars.

where n_e is the electron density expressed in cm^{-3}. This density is determined, in turn, by the stellar winds through:

$$n_e = \frac{\dot{M}_1}{4\pi r^2 v_{\infty,1} \mu m_p},$$ (13)

if m_p is the proton mass.

We have taken the following minimum radio frequencies at which the binary systems have been observed: 1.4 GHz for WR 140 (White & Becker 1995), 327 MHz for WR 146 (Taylor et al. 1996), and 350 MHz for WR 147 (Setia Gunawan et al. 2001a). The derived minimum magnetic fields near the shock front using Eq. (12) are 100 mG for WR 140, 0.6 mG for WR 146, and 0.4 mG for WR 147. The corresponding surface magnetic fields are given in Table 6 as $B_*^{\min}$. These lower limits are quite consistent with our estimates.

During the EGRET observations towards the WR 140 system, it occurred a periastron passage, on 1993.2. The corresponding viewing period (212.0) lasted from March 9 to March 23, 1993, and the measured flux was 25.7 ± 12.7 × 10^{-8} ph cm^{-2} s^{-1}. If we assume that all this flux is due to IC scattering at the colliding wind region, the value of the magnetic field at the shock region must be about 0.16 G, which leads to a stellar surface magnetic field of ~350 G.

6.2. Variability

The size of the non-thermal regions in the WR binaries considered in this research is in the range 10^{14}–10^{15} cm, which is about 3 orders of magnitude larger than the size of the stars. Hence occultation events cannot produce significant flux changes. Variability, instead, can result because of the changing UV photon flux originated in very eccentric orbits and also from changes in the wind outflow. The timescales associated with the first process, however, exceeds the total EGRET observing lifetime by a factor of 2, at least in WR 140, till now the only detectable case. Future GLAST studies might reveal a modulation of the gamma-ray emission with the orbital period for this system. Changes in the winds could affect the injection

Table 6. Stellar magnetic fields.

Star	B_* (G)	$B_*^{\min}$ (G)
WR 140	440	230
WR 146	1200	30
WR 147	50	4

and acceleration rates at the shocks on shorter timescales, but these effects are below the sensitivity of EGRET in the case of WR 140. Long term monitoring with high-altitude ground-based GeV Cherenkov arrays like 5@5 (Aharonian et al. 2001) could be very useful to establish the changing properties of the winds.

6.3. Additional gamma-ray contributions in the region of WR 140

The interstellar matter surrounding the WR 140 system has been studied by means of HI-21 cm radio and IR observations (Arnal 2001 and references therein). Arnal found a minimum in the neutral hydrogen distribution, built by the action of the stellar winds, and estimated an HI mass of the surrounding emission in ~1300 solar masses. The HI void has a major axis of ~11.5 pc and a minor axis of ~8.4 pc. If particle re-acceleration is occurring at the terminal shock of the wind, then the material accumulated in the shell of the HI bubble could be exposed to relativistic proton bombarding yielding an additional contribution to the the total gamma-ray flux measured from 3EG J2022+4317. This is a particularly interesting possibility, since the source is classified as "possibly extended source" in the 3EG catalog.

The γ-ray flux expected from $p - p$ interactions is (Aharonian & Atoyan 1996):

$$F(E > 100 \text{ MeV}) = \frac{1}{4\pi} q_\gamma M_{\text{HI}} \, d^{-2} m_p^{-1},$$ (14)

where q_γ is the gamma-ray emissivity of the medium whose total mass is M_{HI}, d is the distance to the source, and m_p, as before, is the proton mass. The gamma-ray emissivity can be related to the value observed in the vicinity of Earth by $q_\gamma = kq_\odot$. If the proton spectrum near the Earth is similar to the spectrum in the surroundings of WR 140 we can approximate $k \approx k_{CR}$, i.e. the enhancement factor is given by the ratio of cosmic ray densities in the shell and in the solar neighborhood. The latter density is usually taken as ~ 1 eV cm^{-3}, and then $q_\odot(E \geq 100$ MeV$) \approx 2.2 \times 10^{-25}$ (H–atoms)$^{-1}$ (e.g. Dermer 1986). If we consider as reasonable a cosmic ray enhancement in the range $k \sim 10$–100 due to re-acceleration at the wind terminal shock and we adopt the estimate $M_{HI} \sim 1300\ M_\odot$ for the available mass (Arnal 2001), we obtain an additional contribution to the total gamma-ray flux from 3EG J2022+4317 of ~ 1.7–17×10^{-8} ph cm^{-2} s^{-1}. This extended emission could be responsible for the confusion in the EGRET detection. This flux will contribute with a luminosity of ~ 5.7–57×10^{32} erg s^{-1}.

6.4. Remarks on the electron spectrum of WR 147

As we have mentioned in Sect. 3.3 it is not clear that the electron injection spectrum for this system can be represented by a canonical value $p = 2$ as we have assumed for our calculations. Even taken into account the effect of the Compton losses it is not possible to explain the significant steepening observed in the synchrotron flux distribution above 10 GHz (Skinner et al. 1999). The radio spectrum is similar to what would be expected from a monoenergetic electron population. In this case, the spectral distribution of the synchrotron radiation is (e.g. Longair 1997):

$$S(\nu) \propto \left(\frac{\nu}{\nu_c}\right) \int_{\nu/\nu_c}^{\infty} K_{5/3}(\eta)\mathrm{d}\eta, \qquad (15)$$

where $K_{5/3}(\eta)$ is the modified Bessel function and ν_c is the critical frequency near which the emission has its maximum. In the case that the monoenergetic electrons interact with an external photon field, the spectral distribution of the emerging IC radiation will mimic the seed spectrum. With the photon fields considered in this paper, the expected gamma-ray spectrum will be similar to a black body spectrum. In this way, gamma-ray observations of WR 147 with good sensitivity and high spectral resolution can be used to probe the nature of the injected relativistic particle population and to test Skinner et al.'s (1999) proposal of a monoenergetic electron spectrum. Hopefully, GLAST will be able to solve this problem.

6.5. Predictions for upcoming satellites

The gamma-ray fluxes expected at other energy ranges than EGRET's, due to IC scattering of UV photons, for the WR binaries here under consideration, are given in Table 6. It can be seen that some INTEGRAL and GLAST detections can be expected. The continuum sensitivity of INTEGRAL's IBIS instrument is 2×10^{-7} ph cm^{-2} s^{-1} at 1 MeV for an exposure of 10^6 s. GLAST sensitivity at $E > 100$ MeV for one year survey is $\sim 4 \times 10^{-9}$ ph cm^{-2} s^{-1}. High-quality data from these instruments will help to fix the spectral shape of the sources

Table 7. Continuum gamma-ray flux expected at other energy ranges.

| System	F_γ[15 keV–10 MeV][1] (ph cm^{-2} s^{-1})	F_γ[20 MeV–300 GeV][2] (ph cm^{-2} s^{-1})
WR 140	8.3×10^{-4}	1.1×10^{-6}
WR 146	1.2×10^{-4}	8.9×10^{-8}
WR 147	1.2×10^{-3}	9.4×10^{-7}

1: INTEGRAL energy range; 2: GLAST energy range.

in different energy ranges. In particular, notice that IBIS might observe the spectral break predicted at ~ 2.4 MeV for WR 140, whereas GLAST should detect the steepening in the spectrum of WR 147 at energies ≥ 70 GeV.

6.6. Gamma-ray line emission

The winds of WR stars are rich in C and O. In the colliding wind region of a close binary like WR 140, the collision of locally accelerated protons with heavy nuclei may cause the nucleus to break up into lighter fragments that subsequently de-excite producing gamma-ray lines. In particular, the reaction

$$^{16}O + p \rightarrow {}^{12}C^* + \alpha \qquad (16)$$

and the subsequent de-excitation

$$^{12}C^* \rightarrow {}^{12}C + \gamma, \qquad (17)$$
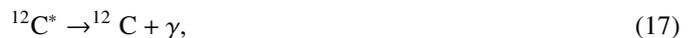
where the gamma-ray photon has an energy of 4.438 MeV. Another important gamma-ray line results from the de-excitation

$$^{16}O^* \rightarrow {}^{16}O + \gamma, \qquad (18)$$

which produces a line feature at 6.129 MeV. Since collective effects can produce observable nuclear interaction gamma-ray lines from the ISM or OB associations (e.g. Ramaty et al. 1979; Parizot et al. 1997), we might ask what is the expected gamma-ray line flux from the systems we are considering here.

The gamma-ray line flux of an object at a distance d is given by:

$$F_\gamma = \frac{1}{4\pi d^2} \int_V \int_E n\ \phi_{CR}(E)\ \sigma(E)\mathrm{d}E\mathrm{d}V. \qquad (19)$$

Here, n is the ambient density of target nuclei, ϕ_{CR} is the flux (cm^{-2} s^{-1}) of energetic particles, and σ is the gamma-ray line production cross section. For the case of WR 140, we estimate a number density of O nuclei of $\sim 5 \times 10^3$ cm^{-3} in the colliding wind region (relative abundance in the stellar wind O/H $\sim 7 \times 10^{-4}$). The volume of the colliding wind region is $\sim 1 \times 10^{41}$ cm^3. Adopting a cross section $\sigma \approx 100$ mbarn and a flux of locally accelerated protons ~ 500 cm^{-2} s^{-1} for energies <100 MeV, we get a 4.438 MeV-line flux at Earth of $\sim 10^{-22}$ ph cm^{-2} s^{-1}, which is many orders of magnitude below the sensitivity of current instruments like INTEGRAL's SPI (e.g. Schönfelder 1999). In the case of the other systems, WR 146 and WR 147, the emission will be even lower because of the lower densities of the colliding wind regions for them. We conclude that, contrary to the case of the continuum

gamma-ray emission, nuclear interaction lines are not observable from *isolated* WR binaries. Collective effects in OB associations, however, might be observable in some cases (Parizot et al. 1997).

7. Conclusions

In this paper we have considered the production of gamma-ray emission in three WR+OB binaries that are well-known non-thermal radio sources. These systems display clear evidence of a colliding wind zone where strong shocks are formed. The existence of a significant synchrotron radio emission from these regions ensures the presence of locally accelerated relativistic electrons, and since the regions are also exposed to strong stellar photon fields, the necessary conditions for inverse Compton production of high-energy photons are fulfilled. We have studied here whether, according to the available multifrequency information, this high-energy emission is detectable with current technology. We conclude that in the case of WR 140, the expected flux is strong enough as to account for an already observed but yet unidentified EGRET source: 3EG J2022+4317. In the case of the WR stars WR 146 and WR 147 the fluxes are below the current detection thresholds, but forthcoming experiments could detect them.

If the existence of gamma-ray emission from early-type stars can be established beyond all observational doubt, the implications for galactic cosmic ray astrophysics could be very important. An important pending issue is what are the maximum energies at which protons could be accelerated by these systems. If re-acceleration takes place efficiently at the terminal shock fronts of the winds, then energies above 100 TeV might be expected. The recent detection of Cyg OB2 association by HEGRA instrument (Aharonian et al. 2002) could be a first step towards the identification of some stellar systems as cosmic ray sources below the so-called knee in the galactic cosmic ray spectrum.

References

Abbott, D. C., Torres, A. V., Bieging, J. H., & Churchwell, E. 1986, ApJ, 303, 239

Aharonian, F. A., & Atoyan, A. M. 1996, A&A, 917, 928

Aharonian, F. A., Konopelko, A. K., Völk, H. J., & Quintana, H. 2001, Astrop. Phys., 15, 335

Aharonian, F. A., Akhperjanian, A., Beilicke, M., et al. 2002, A&A, 393, L37

Arnal, E. M. 2001, AJ, 121, 413

Benaglia, P., & Cappa, C. E. 1999, A&A, 346, 979

Benaglia, P., Romero, G. E., Stevens, I. R., & Torres, D. F. 2001, A&A, 366, 605

Cassé, M., & Paul, J. A. 1980, ApJ, 237, 236

Chapman, J. M., Leitherer, C., Koribalski, B., et al. 1999, ApJ, 518, 890

Churchwell, E., Bieging, J. H., van der Hucht, K. A., et al. 1992, ApJ, 393, 329

Contreras, M. E., Rodríguez, L. F., Tapia, M., et al. 1997, ApJ, 488, L153

Contreras, M. E., & Rodríguez, L. F. 1999, ApJ, 515, 762

Crowther, P. A., Smith, L. F., Hillier, D. J., & Schmutz, W. 1995, A&A, 293, 403

Crowther, P. A. 1997, in The Effective Temperature of Hot Stars, ed. T. R. Bedding, A. J. Booth, & J. Davies (Dordrecht: Kluwer Academic Publishers), 137

Dermer, C. D. 1986, A&A, 157, 223

Dougherty, S. M., Williams, P. M., van der Hucht, K. A., et al. 1996, MNRAS, 280, 963

Dougherty, S. M., Williams, P. M., & Pollaco, D. L. 2000, MNRAS, 316, 143

Dougherty, S. M., & Williams, P. M. 2000, MNRAS, 319, 1005

Drury, L. O. 1983, Rept. Progr. Phys., 46, 473

Eichler, D., & Usov, V. 1993, ApJ, 402, 271

Felli, M., & Massi, M. 1991, A&A, 246, 503

Florkowski, D. R., & Gottesman, S. T. 1977, MNRAS, 179, 105

Hartman, R. C., Bertsch, D. L., Bloom, S. D., et al. 1999, ApJS, 123, 79

van der Hucht, K. A. 2001, New Astron. Rev., 45, 135

van der Hucht, K. A., Setia Gunawan, D. Y. A., Williams, P. M., et al. 2001, in Interacting Winds from Massive Stars, ed. A. F. J. Moffat, & N. St-Louis, ASP Conf. Ser., 1

Ignace, R., Cassinelli, J. P., & Bjorkman, J. E. 1998, ApJ, 505, 910

Jones, F. C. 1968, Phys. Rev., 167, 1159

Koesterke, L., & Hamann, W.-R. 1995, A&A, 299, 503

Lamers, H. J. G. L. M., & Leitherer, C. 1993, ApJ, 412, 771

Leitherer, C., Chapman, J. M., & Koribalski, B. 1997, ApJ, 481, 898

Longair, M. S. 1997, High Energy Astrophysics, vol. 2 (Cambridge: Cambridge University Press)

Maheswaran, M., & Cassinelli, J. P. 1994, ApJ, 421, 718

Mereghetti, S., Tavani, M., Argan, A., et al. 2001, ESA SP-459, 603

Miley, G. K. 1980, ARA&A, 18, 165

Moran, J. P., Davis, S. R., Spencer, R. E., et al. 1989, Nature, 340, 449

Morris, P. M., van der Hucht, K. A., Crowther, P. A., et al. 2000, A&A, 353, 624

Mücke, A., & Pohl, M. 2002, ASP Conf. Ser., 260, 355

Niemela, V. S., Shara, M. M., Wallace, D. J., et al. 1998, AJ, 115, 2047

Parizot, E., Cassé, M., & Vangioni-Flam, E. 1997, A&A, 328, 107

Pollock, A. M. T. 1987, A&A, 171, 135

Ramaty, R., Kozlovsky, B., & Lingenfelter, R. E. 1979, ApJS, 40, 487

Romero, G. E., Benaglia, P., & Torres, D. F. 1999, A&A, 348, 868

Romero, G. E. 2001, in The Nature of the Unidentified Galactic High Energy Gamma-Ray Sources, ed. A. Carraminana, O. Reimer, & D. J. Thompson (Dordrecht: Kluwer Academic Publishers), 65

Schönfelder, V. 1999, in LiBeB, Cosmic Rays and Related X- and Gamma-Rays, ed. R. Ramaty, E. Vangioni-Flam, M. Cassé, & K. Olive, ASP Conf. Ser., 171, 217

Setia Gunawan, D. Y. A., de Bruyn, A. G., van der Hucht, K. A., & Williams, P. M. 2000, A&A, 356, 676

Setia Gunawan, D. Y. A., de Bruyn, A. G., van der Hucht, K. A., & Williams, P. M. 2001a, A&A, 368, 484

Setia Gunawan, D. Y. A., van der Hucht, K. A., Williams, P. M., et al. 2001b, A&A, 376, 460

Skinner, S. L., Itoh, M., Nagase, F., & Zekhov, S. A. 1999, ApJ, 524, 394

Smith, L. F., Shara, M. M., & Moffatt, A. F. J. 1990, ApJ, 358, 229

Smith, L. F., Shara, M. M., & Moffatt, A. F. J. 1996, MNRAS, 281, 163

Taylor, A. R., Goss, W. M., Coleman, P. H., et al. 1996, ApJS, 107, 239

Tompkins, W. F. 1999, Ph.D. Thesis, Stanford University

Torres, D. F., Romero, G. E., Combi, J. A., et al. 2001a, A&A, 370, 468

Torres, D. F., Pessah, M. E., & Romero, G. E. 2001b, AN, 322, 4, 223

Vacca, W. D., Garmany, C. D., & Schull, J. M. 1996, ApJ, 460, 914

Vink, J. S., de Koter, A., & Lamers, H. J. G. L. M. 2000, A&A, 362, 295

Völk, H. J., & Forman, M. 1982, ApJ, 253, 188

Wendker, H. J. 1995, A&AS, 109, 177

White, R. L. 1985, ApJ, 289, 698

White, R. L., & Chen, W. 1995, in Proc. IAU Symp. 163, ed. K. A. van der Hucht, & P. M. Williams (Dordrecht: Kluwer Academic Publishers), 438

White, R. L., & Becker, R. H. 1995, ApJ, 451, 352

Williams, P. M., van der Hucht, K. A., van der Woerd, H., et al. 1987, in Instabilities in Luminous Early Type Stars, ed. H. Lamers, & C. W. H. de Loore (Dordrecht: Reidel), 221

Williams, P. M., van der Hucht, K. A., Pollock, A. M. T., et al. 1990, MNRAS, 243, 662

Williams, P. M., van der Hucht, K. A., Bouchet, P., et al. 1992, MNRAS, 258, 461

Williams, P. M., van der Hucht, K. A., & Spoelstra, T. A. Th. 1994, A&A, 291, 805

Williams, P. M., Dougherty, S. M., Davis, R. J., et al. 1997, MNRAS, 289, 10

Willis, A. J. W., Dessart, L., Crowther, P. A., et al. 1997, MNRAS, 290, 371

Wright, A. E., & Barlow, M. J. 1975, MNRAS, 170, 41